INT. J. REMOTE SENSING, 2003, VOL. 24, NO. 11, 2323–2344

Taylor & Francis
Taylor & Francis Group

Resolution dependence of infrared imagery of active thermal features at Kilauea Volcano

H. GAONAC'H

Centre GEOTOP, Université du Québec à Montréal, C.P. 8888, succursale
Centre-Ville, Montréal, Québec, H3C 3P8, Canada;
e-mail: gaonac'h.helene@udam.ca

S. LOVEJOY

Physics Department, McGill University, Montreal, QC, H3A 2T8, Canada

and D. SCHERTZER

Laboratoire de modélisation en mécanique, Université Pierre et Marie Curie,
Paris cedex 05, 75252 France

(*Received 16 August 2000; in final form 27 November 2001*)

Abstract. Standard methods for monitoring and analysing thermal volcanic fields have difficulty taking into account the large dynamical range of temperatures and radiative fluxes which occur over enormous ranges of spatial scale. They typically are either qualitative or if quantitative, only in the identification of a small number of 'anomalies' mapped at coarse resolutions. We argue that remote sensing of such fields invariably involves averages over small 'hot spots', and that the results depend sensitively and systematically on the space–time resolutions of the sensors. In order to overcome these difficulties and to provide resolution and hence observer-independent characterizations, we use various statistical scaling analysis techniques. We demonstrate their advantages on images of various volcanic features in the thermal infrared spectral region (8–12 μm) acquired above the active part of Kilauea volcano in December 1995 using a helicopter-borne infrared (IR) camera. We first demonstrate the scaling of the thermal remotely sensed radiances using energy spectra and show they are of the power law form $E(k) \propto k^{-\beta}$, where k is a spatial wavenumber in the image, and β is a scale-invariant spectral exponent. Over the range of over 10^4 in scale (from 4 cm to 775 m) and for a variety of volcanic structures, we find $\beta \approx 2.0 \pm 0.1$. Moreover, the thermal fields show multiscaling behaviour characterized by universal multifractal parameters; we find the degree of multifractality $\alpha \approx 1.7 \pm 0.2$, the codimension of the singularity contributing to the mean $C_1 \approx 0.14 \pm 0.04$ (characterizing the sparseness of the mean gradients) and finally the conservation parameter $H \approx 0.65 \pm 0.05$, which largely determines the roughness (scale by scale) of the radiance field. These three universal multifractal parameters characterize the resolution dependence of both low- and high-radiance regions over the entire range of spatial scales studied. We compare and contrast these parameters with those (found in other studies) of the topography and volcanic albedo.

We also propose a new way to enhance the thermal volcanic anomalies of daytime images through filtering. This is done by shifting the H values (power

International Journal of Remote Sensing
ISSN 0143-1161 print/ISSN 1366-5901 online © 2003 Taylor & Francis Ltd
http://www.tandf.co.uk/journals
DOI: 10.1080/01431160210164253

law filtering) to those of the observed night-time images and produces 'simulated' nocturnal images with essentially the same (scale by scale) statistics; it is a kind of scale-invariant contrast enhancement. Finally, we show how knowledge of the scaling statistics can be used to determine the statistical expectation of large-scale thermal fluxes conditioned on the corresponding large-scale temperatures.

The multifractal properties demonstrate the necessity of explicitly taking into account the (essentially subjective) sensor resolution when interpreting and modelling active volcanic thermal fields. It underlines the need to properly characterize the non-classical geostatistics of the radiance field before interpreting the latter in terms of temperatures and anomalies.

1. Introduction

1.1. *The resolution dependence of remotely sensed volcanic data*

Active volcanic areas require intensive surveillance. Among the different methods available for both public security and scientific purposes, thermal remote sensing is particularly suitable. The spatial/temporal activity of certain volcanoes, such as Kilauea (Hawaii), are routinely monitored (e.g. Realmuto *et al.* 1992, 1997, Flynn and Mouginis-Mark 1994, Flynn *et al.* 1994, Harris *et al.* 1998).

Remotely sensed thermal data may be collected from the ground, air or space. They may be highly 'local' small-scale values (e.g. temperatures estimated with an infrared pyrometer averaged at centimetre resolutions), or large-scale images of individual volcanoes (e.g. at resolutions of 30–120 m for the various channels of Landsat satellite images) or even larger scales of entire volcanic regions (e.g. at resolutions of 1–4 km, GOES data). The infrared region of the electromagnetic spectrum is particularly well suited for surveying surface lava flows or flow fields, lava tubes, or lava lakes such as those present at Kilauea. In this context, the Landsat Thematic Mapper (TM) Short Wavelength Infrared (SWIR) sensors (1.55–1.75 μm and 2.08–2.35 μm) are mainly used for mapping active flow units while Landsat TM Thermal Infrared (TIR) band (10.42–12.42 μm) mostly reveals cooling lava flows that are days or weeks old. The growing accessibility of these data has stimulated new research for combining information acquired at different spatial, temporal and spectral resolutions.

Most studies to date have aimed at developing applications to urgent problems of monitoring volcanoes; there has been comparatively little attention paid to fundamental issues associated with the extreme variability of the observed radiance fields themselves. Indeed, virtually all applications are based—implicitly or explicitly—on assumptions of sub-pixel homogeneity. For example, infrared based studies are almost invariably limited to estimates of the spatial distributions of the areas or of the maximum values of thermal anomalies at unique spatial resolutions or of their general developmental tendencies, the latter particularly in conjunction with local *in situ* thermal measurements (e.g. Oppenheimer *et al.* 1993b, Harris and Stevenson 1997, Wooster and Kaneko 1998, Flynn *et al.* 2000). This includes thermal and emissivity mapping of volcanic regions as well as estimates of total thermal fluxes (e.g. Realmuto *et al.* 1992, Kahle *et al.* 1988, Glaze *et al.* 1989), the detection of qualitative volcanic features (e.g. Oppenheimer 1991, Flynn *et al.* 1994, Gaonac'h *et al.* 1994, Harris and Stevenson 1997, Harris *et al.* 1997) and the estimate of averaged volcanic properties such as lava effusion rates in Harris *et al.* (1998).

A key advantage of remotely sensed data with respect to traditional *in situ* sources is its ability to give a synoptic view of the entire thermal field (including anomaly structures). However, their interest is devalued unless the full available range of space/time scales (and hence, surface temperatures and radiative fluxes) is exploited. In this regard, a particularly extreme tendency has recently developed in which the data resolution is so low that the entire anomaly is reduced to a tiny fraction of a single pixel; relative increases or decreases in the radiances at this single pixel is then used as an indicator of the relative activity of the volcano. For example, Harris and Stevenson (1997), Wooster and Kaneko (1998) and Harris *et al.* (2000) deduced the intensity of the volcanic activity with data acquired at very low resolution (1 km for AVHRR images, 4 km for GOES) or with very poorly known spatial distributions (e.g. local ground-based measurements). While these data have resolutions of the order of 1 km^2, the underlying temperatures (and hence black body radiances) are highly variable over millimetre- or centimetre-scale regions.

The resolution problem has motivated attempts to take this strong heterogeneity into account through 'dual-band' methods (first applied to volcanic targets by Rothery *et al.* 1988) which consists of partitioning the sub-pixel structures into homogeneous sub-regions and using different wavelength information to improve temperature estimates at the pixel scale. While these methods partially address the problem, they only provide marginal improvements in the effective spatial resolution since with n wavelengths, the homogeneity assumption must still be made over at least a fraction $1/n$ of the pixel whereas the true homogeneity scale may be 10^6 (or more) times smaller (e.g. 1 km/1 mm). Such approaches do not therefore significantly modify the sub-pixel resolution problem. In this paper, we therefore rather aim to systematically statistically characterize the radiance fields themselves over as wide a range of scales as possible; this is a necessary first step in understanding their non-classical geostatistical variability (Lovejoy *et al.* 2001). The idea is to replace sub-pixel homogeneity assumptions by heterogeneity assumptions, assuming that the observed large-scale heterogeneity continues statistically to very small sub-pixel scales. Understanding the resulting resolution dependence is urgent if we are to improve the interpretation and modelling of highly variable fields such as the thermal volcanic field; this is especially true if we seek to combine remotely sensed and conventional data in a Geographic Information System (GIS, which involves data taken at quite different resolutions).

The limits of the standard homogeneity based approaches in understanding volcanic dynamics are particularly evident when considering the important question of heat fluxes. The heat fluxes through the surface of active volcanoes (during an eruption or between eruptions) depends on the internal dynamics of the volcano as well as on the inter-relations between the volcano and the atmosphere. The geothermal and solar heat sources are accompanied by radiative and convective heat sinks between the ground and the air (e.g. Gaonac'h *et al.* 1994) each of which has a highly heterogeneous space/time structure over a wide range of scales. Therefore, quantifying the spatio-temporal distribution heat fluxes of a volcano is a much more demanding task than the regular monitoring of the volcano. On the one hand it requires a conceptual framework capable of handling the huge (non-classical) variability, on the other hand it provides the inputs necessary for quantitative volcanic modelling.

1.2. *Scale invariance and strong nonlinear variability*

Many geological and geophysical phenomena including volcanoes are the result of highly nonlinear dynamical processes leading to heterogeneous structures (e.g. lava flows, gas vesicle size distributions, fractures) and highly variable fields (e.g. visible radiance, topography). These fields display (1) a strong variability of the field values (radiance, altitudes, etc.) at a fixed scale as well as (2) for a given intensity level, a large spatial variability over a wide range of spatial scales. More precisely it is typically found that for a given spatial resolution, wide ranges of intensity exist while each intensity threshold defines a different fractal set characterized by different exponents (e.g. fractal dimensions). The simplest hypothesis to quantify such variability, is to suppose that the same basic nonlinear mechanism acts over a wide range of scales, i.e. that the variability (statistics) obey scale-invariant symmetries (Gaonac'h *et al.* 1992, 1996a, b, Dubois and Cheminée 1993, Bruno *et al.* 1994). Any other assumption would involve more than one mechanism, and would only be justified if a single mechanism was first shown to be inadequate. Except in the special (unrealistically symmetric) case where the scale invariance is isotropic (self-similar) it will generally be anisotropic ('generalized scale invariance'—GSI). The morphology and texture of structures will therefore generally change with scale even though the basic generator is scale invariant. GSI shows that the assumption that structures whose shape/appearance changes with scale do not necessarily require distinct underlying mechanisms; this must be investigated by systematic scaling analyses. In scaling regimes, the significant statistical properties are observer/resolution independent exponents, such as those determining the area of the lava flow field (Gaonac'h *et al.* 1992, Bruno *et al.* 1994, Bruno and Taylor 1995).

One type of scaling which is now well known is the fractal geometry of scale-invariant geometric sets of points. The scaling is characterized by one or a small number of scale-invariant exponents, typically the fractal dimension. However, when we deal with a scaling (mathematical) field (e.g. the temperature, which has a value at each space/time point) we generally have multiscaling behaviour whose scale-invariant exponents are functions, not numbers, corresponding to an infinite hierarchy of fractal dimensions (for example, different fractal dimensions for each line of constant altitude). Recent studies have demonstrated the multifractal aspect of many remotely sensed fields (Lovejoy and Schertzer 1995, Schertzer and Lovejoy 1995, Schmitt *et al.* 1997, Pecknold *et al.* 1997, Laferrière and Gaonac'h, 1999, Lovejoy *et al.* 2001). The generic multifractal processes are cascades (e.g. Schertzer *et al.* 1997); the corresponding cascade models are based on a succession of multiplicative steps in which large 'parent' structures evolve into smaller 'daughter' ones with the large scale multiplicatively modulating the small-scale intensities. An important consequence useful for applications is that we may statistically extrapolate the multifractal fields to resolutions which are not otherwise accessible to us—either at larger scales (upscaling, aggregation), or at sub-pixel scales (downscaling, disaggregation), see §6.1 and Lovejoy *et al.* (2001) for some explicit formulae for doing this.

In this paper, we analyse remotely sensed thermal images of the active part of Kilauea volcano (figure 1), acquired in December 1995 from a helicopter with a thermal infrared video camera. These data (see §2) from a highly variable volcanic field reflect the nonlinear dynamics related to lava emplacement at the surface of the volcano. We present different statistical methods to quantify this variability over a range of scale of $\approx 10^4$. Over this range, a common scaling behaviour was found to describe all the various observed volcanic features. We characterize the multiscaling exponents which define the statistical moments of the observed volcanic fields at each resolution. We then compare the corresponding multifractal parameters with

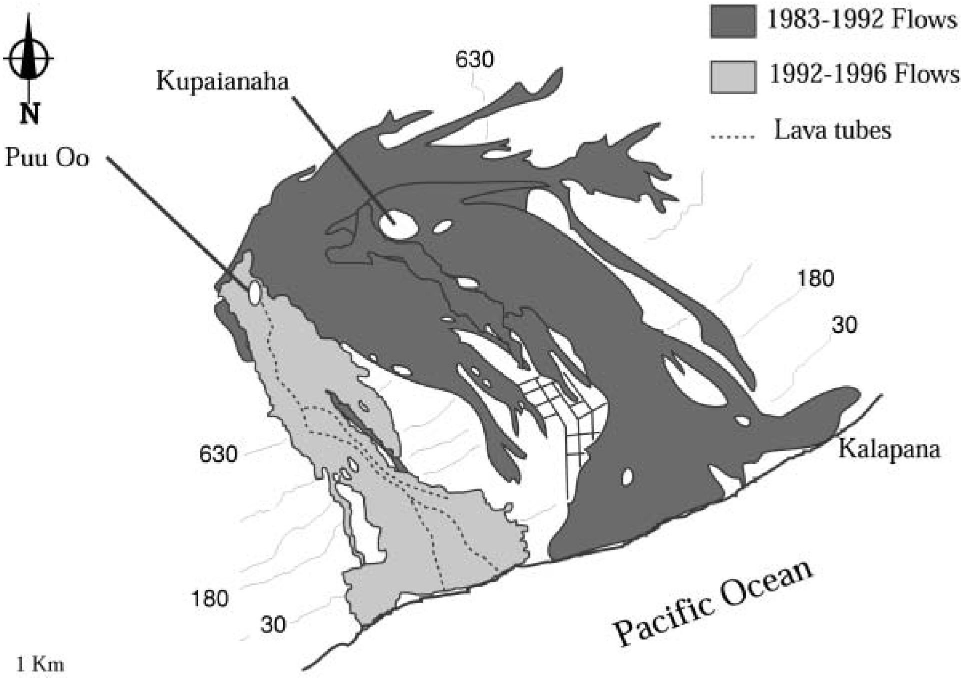

Figure 1. Map of the Kilauea area where volcanic activity was present in December 1995. Contours are in metres.

other volcanic and geophysical fields, and discuss the implications for the understanding of volcanic phenomena as well as for estimating the total flux over a heterogeneous area. We finally applied the multiscaling properties to enhance the thermal volcanic anomalies through filtering of the daytime images.

2. Data acquisition

Analogue and digital video pictures were acquired with an Inframetrics 760 model thermal infrared scanning radiometer in the thermal infrared (TIR) wavebands (3–5 μm, 8–12 μm). Six of the 18 analysed images are shown in figure 2. These bands correspond to atmospheric windows where the atmospheric transmissivity is high. This is especially true for the 8–12 μm band since data acquired from airborne sensors are free of the absorption due to O_3, which adversely affects the corresponding satellite images. In contrast, the 3–5 μm band has significant absorption at 4.2 μm due to water vapour. It also suffers from daytime contamination from solar reflection. For these reasons, most images were acquired in the 8–12 μm band. In addition, for studying geothermal anomalies, the optimum local time of day was $\approx$6 a.m., when the ground is cool enough to be less affected by solar heating effects. This acquisition time provides the highest radiative contrast between active and non-active volcanic areas. For statistical day/night comparisons, some data acquired during daytime are also included as well as data obtained in the 3–5 μm region. Data were collected from a helicopter at variable elevations above the ground implying a range of image resolutions varying from 4 cm to 6 m per pixel (table 1 and figure 4).

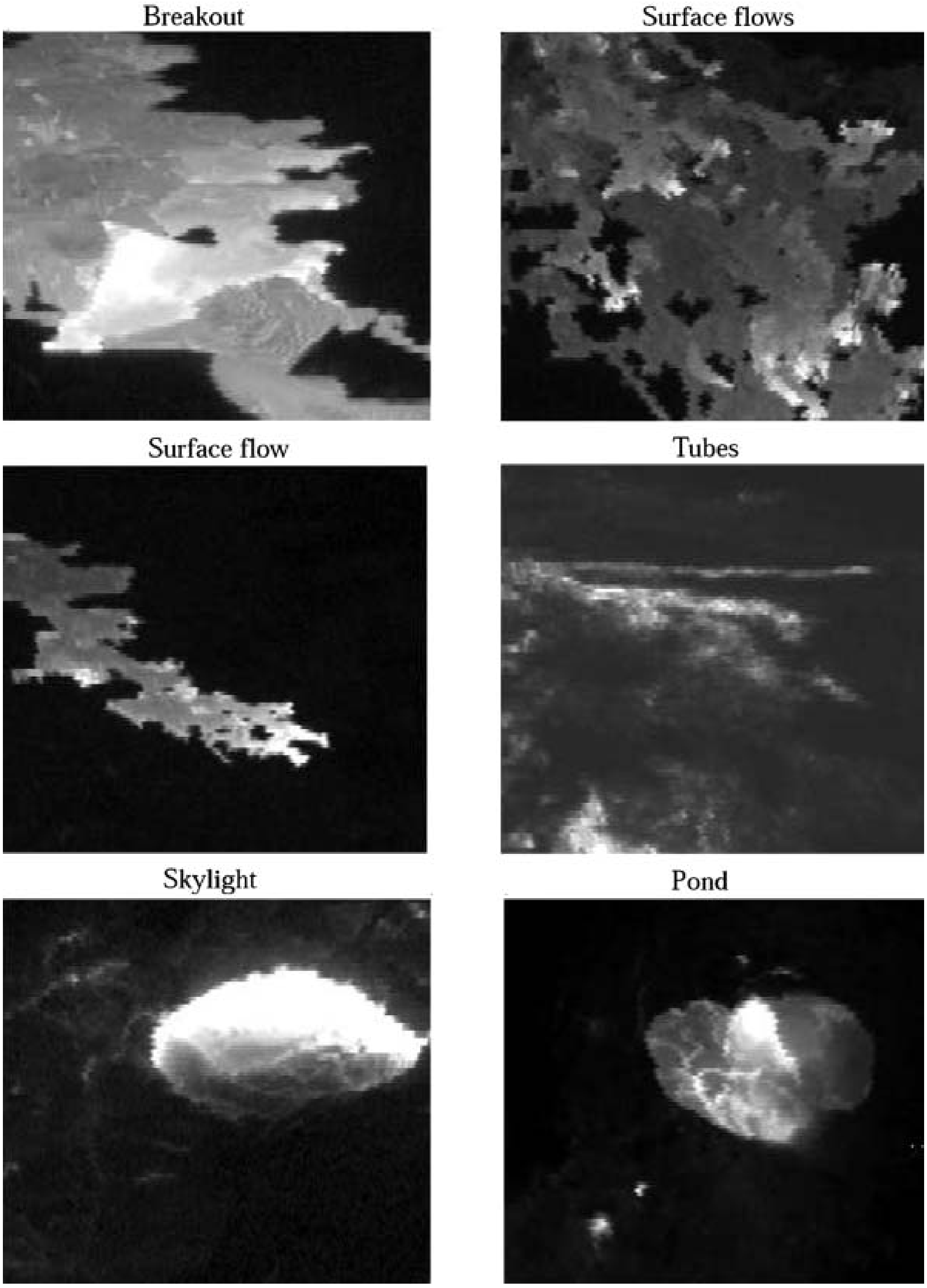

Figure 2. Examples of volcanic features observed in the thermal infrared region and analysed in this study. The highest radiative infrared intensities are in white. The images have been enhanced for visualization only.

Table 1. Characteristics of the numerical images shown in figure 2.

Volcanic features	DN range	Estimated T range (K)	Resolution (m)
Breakout	12–245	350–1020	0.6
Surface flows	4–139	350–820	6.0
Surface flow	21–150	390–730	1.4
Tubes	22–196	300–350	2.5
Skylight	23–255	400–932	0.04
Pond	8–229	350–1050	0.4

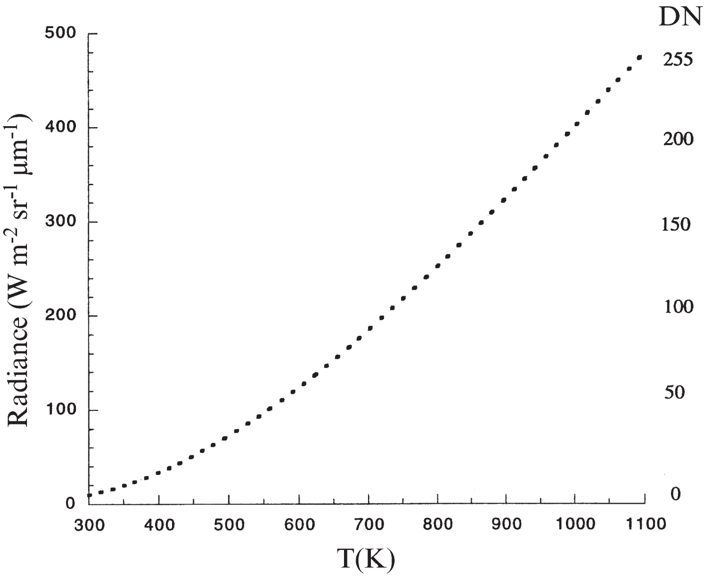

Figure 3. Diagram of the thermal emitted radiance of the 8–12 μm region as a function of the temperature for the surface flows.

The images were acquired subvertically to minimize geometric distortions. Neither geometric corrections nor atmospheric corrections were applied; the surface is relatively flat and the viewing distances were rather small. In any case, the effect of geometric corrections is mostly confined to the highest spatial frequencies (see Harvey *et al.* 2002).

Images were recorded as digital numbers (DN) with 8 bit dynamic range with 256×208 pixels per image. Each DN value is nearly linearly proportional to the spectral radiance $R_{\lambda}(T)$ received at the airborne detector. Spectral radiances are related to temperatures through the Planck function. In each image, the range of temperatures is such that the relationship between the radiances and the radiative temperatures (provided by the video pictures) can be approximately considered as linear (see, for example, figure 3). For simplicity we therefore preferred to analyse the raw radiance values linearly related to DN values and did so on 128×128 pixel images. In any event, we analysed the statistical properties of field gradients which are not sensitive to the comparison between images acquired with various dynamic and temperature ranges.

3. Energy spectrum

In most images, the DN probability distribution shows a highly non-gaussian behaviour, with a long tail towards the large DN values. The thermal radiance fields therefore cannot be objectively characterized (independently of the sensor resolution) by a unique temperature value such as the averaged DN or the maximum DN; the whole range of DN values represents the effects of dynamic radiative losses of the surface of an active volcanic field.

A convenient analysis method sensitive to scale breaks is the energy spectrum. Although the spectrum is only a second-order moment (variance per wavenumber), it is nevertheless a useful analysis technique. A complete statistical characterization requires the analysis of all the moments; this will be performed later. Following standard usage in the turbulence literature, the Fourier spectral energy density $E(k)$ presented in this paper is the angle-integrated, ensemble-averaged, squared modulus of the Fourier transforms of the images where k is the wave number (modulus of the wavevector). It gives the mean contribution to the variance from all structures with wavenumber between k and $k+dk$. An (isotropic) scale-invariant field will be characterized by an energy spectrum such as:

$$E(k) \propto k^{-\beta} \tag{1}$$

where β is the scaling exponent[1], hence in scaling regimes $\log E$ against $\log k$ is linear[2].

Figure 4 shows the energy spectrum $E(k)$ for various Hawaiian thermal infrared fields. Several conclusions can be drawn:

1. We may define a common scaling trend over the range of scales going from ≈ 8 cm (corresponding to $k = 10^{1.10}$ cycles/m) to ≈ 770 m (corresponding to $k \approx 10^{-2.88}$ cycles m^{-1}) with a scale-invariant exponent $\beta \approx 2.0 \pm 0.1$. Large and small thermal radiative intensities are thus related by a scaling law over a range of scales of at least roughly four orders of magnitude. Because β is defined as an ensemble-average quantity and multifractal fields are highly intermittent, we may expect large fluctuations from one image to another, especially when images are small (128×128 pixels). The number of saturated pixels in our images was sufficiently small that we did not observe any significant difference in β for fields having saturated pixels (DN = 255).
2. In figure 4 we note breaks in the scaling for each individual image at the highest k values (primarily the highest factor 2 in wavenumber). These are artefacts due to undersampling by the Inframetrics imaging radiometer (leading to an aliasing effect) combined with the presence of some noise in the signal. The spurious nature of these breaks is particularly obvious when each spectrum is compared to the common systematic scaling over the whole series of analysed images.
3. We observe a tendency for the value of β to increase between pre-dawn and daytime images (table 2). Since a higher β value implies a smoother field, this could be explained by solar surface heating during the day which reduces the thermal contrasts (at night all of the non-active volcanic regions are at nearly

---

[1] In solid earth applications, the angle integration is often replaced by angle averaging; the result then depends on the dimension of the sample. In addition to constants such as 2π, there is an extra k^{d-1} factor where d = dimension of space ($d = 2$ for images).

[2] Strictly speaking, this is only true of isotropic scaling. Anisotropy—even if it is scaling—will lead to a break in the isotropic spectrum.

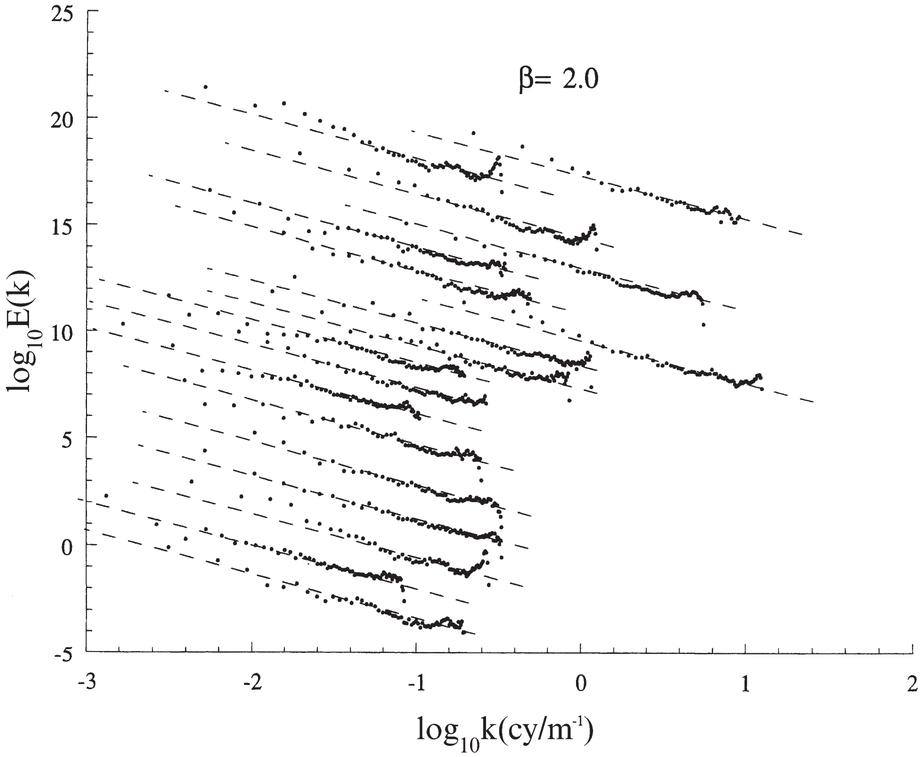

Figure 4. Spectral energy density $E(k)$ as a function of the radial wave number k (cycles m^{-1}) for all the analysed images. A common $\beta=2.0$ (± 0.1) slope can be defined for all the images. For clarity, the data have been vertically shifted. The overall scaling goes from 0.08 m ($k=10^{1.10}$ cycles m^{-1}) to 770 m ($k=10^{-2.88}$ cycles m^{-1}).

Table 2. Comparison of the statistical β parameters for the various groups of Hawaiian images acquired in December 1995.

Spectral region	Date	β
8–12 μm	6 am 20 December 1995	2.00
8–12 μm	4 pm 19 December 1995	2.20
3–5 μm	4 pm 19 December 1995	2.20

the same background DN values), although it is significant that this change in contrast affects all scales, not just a narrow range.

4. We do not observe any significant statistical differences (table 2) between the values obtained in the 3–5 μm and in the 8–12 μm bands. We may easily explain this result as emission from the active volcanic surface in higher or lower ranges of temperatures, respectively.

4. Multiscaling

4.1. *Multiplicative cascades*

Since the radiative intensity measured by Landsat represents a mean value over a 30 × 30 or 120 × 120 m pixel in the thermal infrared band, a 10°C thermal anomaly from a Landsat thermal band may be due to a very small anomaly of hundreds of degrees (°C) at metric or sub-metric resolutions. The dual (or multi) band method (e.g. Rothery *et al.* 1988, Oppenheimer *et al.* 1993a) acknowledges the problem and models it with homogeneous sub-pixel components; for example, in the dual band method, a 'hot' component corresponding to a magmatic temperature and a 'cold' component identified as a background temperature. Harris *et al.* (1998) suggest a more complex combination of three, four or more sub pixel components (the 'sharpening method'). As mentioned earlier, an n band method of this sort effectively increases the resolution by only a factor of order n since homogeneity assumption is required over at least some sub-regions of the order of $1/n$ of the pixel. We are therefore far from the resolution necessary to resolve the sub-pixel structures of inhomogeneous areas which may theoretically be millimetric. We prefer to consider—in a theoretically consistent way—the observed available remote radiance (in the present study the TIR spectral radiance) as an average value of a 'sub-thermal radiance field' which is observer-dependent, and exploit the scaling properties to statistically extrapolate over the entire range. Indeed, the multifractal framework is ideally suited to statistical 'downscaling' or 'disaggregation': for some recent relevant results on multifractal statistical scale extrapolation (conditional statistics), see Lovejoy *et al.* (2001).

The generic multifractal process is the multiplicative cascade in which variability is built up scale by scale as the cascade proceeds from large to small scales. The result of such cascades is that the temperature of the field—at each observed pixel—will vary according to the resolution of observation; a scaling cascade developed over a range of scales of ratios λ, by a power law function relating the probability distribution[3] of the intensities of the field versus the scale ratio:

$$\left.\begin{array}{r}\Pr(\varepsilon_\lambda \geqslant \lambda^{\gamma}) \approx \lambda^{-c(\gamma)} \\ \varepsilon_\lambda = \lambda^{\gamma}\end{array}\right\}, \lambda > 1 \tag{2}$$

where ε_λ is the intensity of the field (described here as an absolute DN gradient) at the scale ratio λ (ratio of the larger outer scale L to the smaller intermediate scale l), γ is the order of singularity, $c(\gamma)$ its associated co-dimension function, 'Pr' indicates 'probability' and the sign '$\approx$' indicates equality to within slowly varying (sub-exponential) factors (such as $\log \lambda$). λ^{γ} is a threshold defining the regions associated with singularities γ; a particular threshold—defined, for example, to identify a thermal volcanic feature such as lava 6 hours old (Harris *et al.* 1998)—will thus depend on the resolution of observation (λ) in a power law way. If $c(\gamma) < d$ ($d =$ the dimension of space $= 2$ here), the regions defined in this way will be fractal sets with fractal dimension $d(\gamma) = d - c(\gamma)$.

An additional feature of multifractal processes is that their small-scale limit ($\lambda \longrightarrow \infty$) is highly singular; this leads to wild variability which is only partially reduced by spatial averaging at a given scale. To distinguish the properties of the (theoretical) multifractal process developed over a finite range λ, and the (even) more variable process continued over an infinite range (the small-scale limit) and then averaged to the same scale, Schertzer and Lovejoy (1987) introduced the expressions 'bare' and 'dressed', respectively. As already stressed in Laferrière and Gaonac'h

---

[3] Strictly speaking, this is equal to 1 minus the usual cumulative probability distribution function.

(1999), the statistics of the dressed cascade are more variable than the bare statistics: the dressed properties take into account the small-scale variability as well as that due to the large scales. They generally imply interesting non-classical extremes associated with the divergence of high order statistical moments and 'self-organized criticality'.

Rather than analysing their probability distributions, the multifractal aspect of fields can also be analysed through their various statistical moments, which in general are 'multiscaling':

$$\langle \varepsilon_\lambda^q \rangle \propto \lambda^{K(q)} \tag{3}$$

where q represents the order of the moment and $K(q)$ the multiscaling exponent. The statistical properties of the process can be specified by either $K(q)$ or $c(\gamma)$; the two are related by a Legendre transform (Parisi and Frisch 1985).

4.2. *Characterization of multifractal universality*

Whereas many different parameters may be needed to define a scaling geophysical process via its $K(q)$ or $c(\gamma)$ functions, it has been argued that in many cases only a few numbers are necessary to statistically characterize the multifractal process (Schertzer and Lovejoy 1987, 1991, Schertzer *et al.* 1997). This is due to the existence of stable, attractive multifractal processes, i.e. when a nonlinear dynamical mechanism is repeated scale after scale or when nonlinear 'mixing' prevails many such processes, then many of the details get 'washed out'; the result generally depends on very few of the details. This is exactly analogous to the drunkard's walk problem: under rather general assumptions about the individual steps the drunkard makes, the result will be a gaussian Brownian motion. In such a 'universal' multiscaling, the $K(q)$ function can be expressed with two universal parameters:

$$K(q) = \frac{C_1}{\alpha - 1}(q^\alpha - q) \qquad \alpha \neq 1 \tag{4a}$$

$$K(q) = C_1\, q \log(q) \qquad \alpha = 1 \tag{4b}$$

where the Lévy index α indicates the degree of multifractality of the process and varies between 0 and 2. $\alpha = 0$ corresponds to the monofractal 'β model' while $\alpha = 2$ represents a 'log normal' multifractal (although due to the 'dressing', the statistics are not exactly log-normal). C_1 represents the fractal co-dimension of the mean and quantifies the sparsity of the singularity (the scale-invariant intensity) contributing to the mean of the field. For a non 'degenerate' process, $0 \leqslant C_1 \leqslant d$ where d is the dimension of the space. C_1 close to 0 implies that the structures dominating the mean are fairly homogeneously distributed, while a C_1 value close to d is associated with a few isolated large 'spikes' contributing to the mean.

The universal multifractal parameters are conveniently estimated by a method proposed by Lavallée *et al.* (1993), the double trace moments technique (DTM). This method involves the use of moments with two different statistical orders, q and η at different resolutions λ:

$$\langle (\varepsilon_\Lambda^\eta)_\lambda^q \rangle \approx \lambda^{K(q,\eta)} \tag{5}$$

The notation in equation (5) means that various η powers of the intensity ε_Λ at each pixel of the field, measured at the highest available resolution Λ^{-1}, are taken systematically spatially averaging them to lower resolution (λ^{-1}) and finally averaging the q^{th} moment of the result, repeating for lower and lower resolutions. Comparing equations (3) and (5), we see that $K(q)=K(q,1)$. More generally, we obtain: $K(q,\eta)=K(q\eta)-qK(\eta)$, which applied to $K(q)$ of the universal form equation (4) leads to:

$$K(q,\eta)=\eta^{\alpha}K(q,1)=\begin{cases}\dfrac{C_1}{\alpha-1}\eta^{\alpha}(q^{\alpha}-q) & \alpha\neq 1\end{cases} \tag{6a}$$

$$K(q,\eta)=\eta^{\alpha}K(q,1)=C_1\eta q\log(q) \qquad \alpha=1 \tag{6b}$$

α is estimated as the slope of the scale-invariant function $K(q,\eta)$ on a log–log plot, while C_1 corresponds to the intercept. In practice, increasing the η values leads to statistics increasingly dominated by the higher intensities of the field: high ε_Λ values are enhanced compared to low ones. Relevant geophysical examples of the DTM technique are Lavallée *et al.* (1993) and Laferrière and Gaonac'h (1999). A cascade multiplicatively modulates a flux from large to small scales; on average the latter is conserved (scale by scale). However, observables are typically not conserved; in the simplest fractionally integrated flux (FIF) model (Schertzer *et al.* 1997) these are obtained by fractionally integrating (power law filtering) the flux (exponent H). Because $K(2)>0$, a conservative field ($H=0$) will necessarily have $\beta<1$. On the other hand, $\beta>1$ observed for analysed thermal fields (see §3) implies $H>0$; hence non-conservative processes ($H>0$).

The resulting non-conservative observed thermal radiance field (R_λ) is related to a conservative field ε_λ as:

$$\Delta R_\lambda=\varepsilon_\lambda^{a}\lambda^{-H} \tag{7}$$

where H is the 'Hurst' parameter characterizing the degree of non-conservation of the analysed field otherwise its roughness. Since the energy spectrum is the square of the Fourier modulus, H is related to the Fourier scaling exponent via $\beta=1-K(2)+2H$. Hence, non-conservative fields have to be transformed through power law filters (differentiated) into a conservative field before estimating its multiscaling properties (Lavallée *et al.* 1993). It turns out that an approximation adequate for most purposes is to transform the field intensities by field gradients such as:

$$|\Delta R(i,j)|=\sqrt{[R(i+1,j)-R(i-1,j)]^2+[R(i,j+1)-R(i,j-1)]^2} \tag{8}$$

The indexes are, respectively, the horizontal and vertical coordinates going from 1 to 128. This is a numerical approximation to an (isotropic) first-order derivative which reduces H by 1. As long as the resulting $H<0$, then α and C_1 will be appropriately estimated for a conservative field.

4.3. *Highly multifractal thermal field*

The analyses were performed on 128×128 pixel images with a factor 2^8 of dynamic range (8 bit digitization). As mentioned in §3, the data show an aliasing effect near the resolution of acquisition (figure 4). We hence degraded the resolution of the images by a factor of 2 and compared their multiscaling behaviour with those of the original images. Whereas the energy spectra are affected by low quality resolution such as the aliasing effect, the double trace moment (DTM) method is fairly insensitive to the relatively small amount of aliasing present. In order to preserve the largest possible range of scales, we therefore performed the DTM analyses on 128 × 128 pixel images. Figure 5 shows the multiscaling observed for an image where an active surface flow is present. For each η value (enhancing various distinct intensities of the field) and for the moment $q = 1.5$ (a moment somewhat arbitrarily chosen between the mean, $q = 1$ and the variance, $q = 2$), the scaling behaviour is observed through statistical moments over a range of scales of nearly 128 (the size of the image) and characterized by the linear trend in this $\log_{10}$–$\log_{10}$ diagram with a slope $K(q, \eta)$. The multifractality is exhibited by the variation of the scale-invariant function $K(q, \eta)$ as a function of the tuning η whereas a monofractal field $\alpha = 0$ will lead to constant $K(q, \eta)$ for varying η, fixed q. Note that a potential problem with 8 bit data is that they can exhibit anomalous low α values. This is a consequence of the narrow dynamic range characterizing these images which generally implies a large number of spurious zero gradients (i.e. zero gradients which are purely due to the inadequate 8 bit discretization; see, e.g. Pecknold *et al.* 1997, Laferrière and Gaonac'h 1999). This leads to a flattening of $K(q, \eta)$ at low η values and an abnormal flat trend of the multiscaling of $\langle (\varepsilon_\Lambda^\eta)_\lambda^q \rangle$ as a function of λ. In our case, this was not a major problem since zero gradients of our selected images covered less than 10% of the image.

Figure 6 shows that the variation of $K(q, \eta)$ versus η may be simply expressed (see equation (6a)) with two universal values where α is close to 1.7 (± 0.2), demonstrating the high degree of multifractality of the volcanic thermal field from 4 cm to 770 m: since α is close to the maximum (≈ 2), singularities of all orders contribute significantly to the process (at the other extreme, $\alpha = 0$, which may imply $K(q, \eta)$ independent of η, only singularities with a unique fractal dimension are important, the process is 'monofractal'). The C_1 parameter is estimated from figure 6 by the

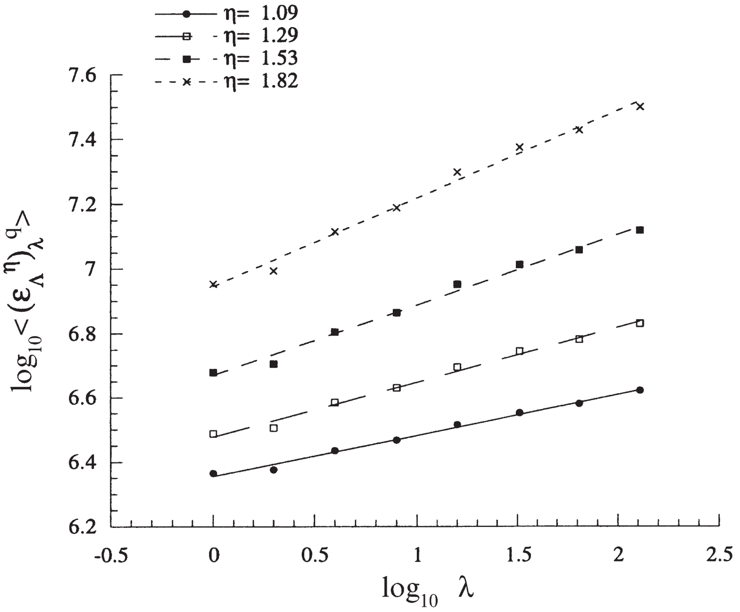

Figure 5. $\log_{10}(\varepsilon_\Lambda^\eta)_\lambda^q$ versus $\log_{10}\lambda$ for various η values and $q = 1.5$ for the surface flow image. For each η intensity defined at the highest resolution, the degradation of the statistical moments of order $q = 1.5$ over the range λ follows a power law (linear in $\log_{10}$–$\log_{10}$ plot) function with distinct slope.

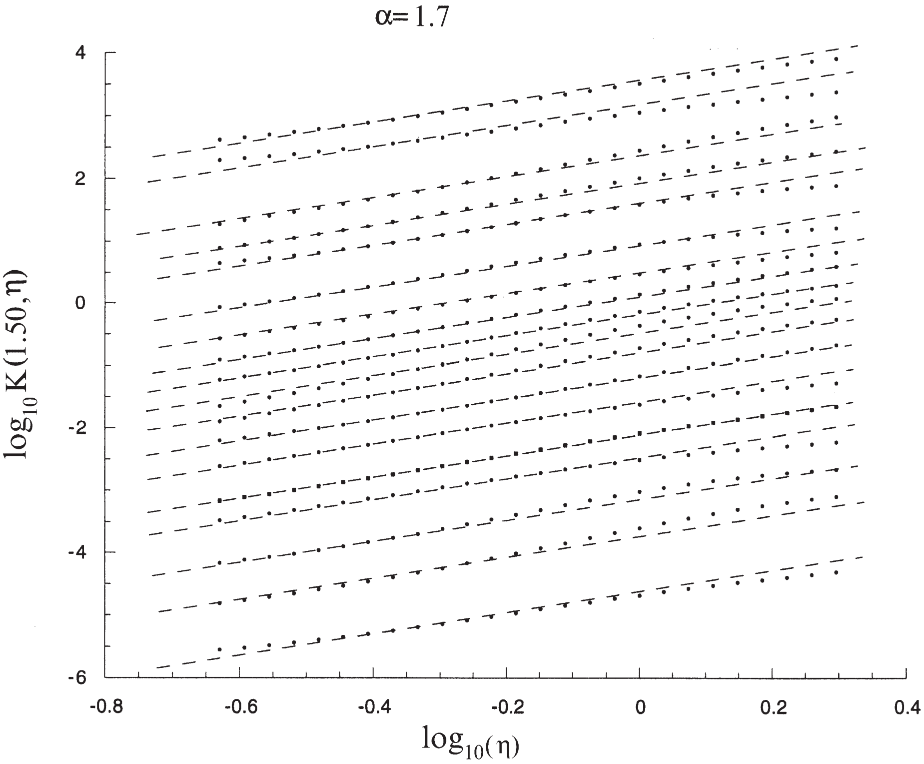

Figure 6. $\text{Log}_{10}K(1.5, \eta)$ versus $\log_{10}\eta$ for the images presented in figure 2, exhibiting the universal multifractality of the data over approximately $\eta = 0.21$ to $\eta = 2$. The variation of slopes as defined in figure 5 can be described by a common linear trend with a slope $\alpha = 1.7$ (± 0.2) for all the volcanic features. The dashed lines are reference lines with slopes 1.7. The data are offset in the vertical for clarity.

intersection of the linear part of the data with the line $\log \eta = 0$. The overall average C_1 is close to 0.14 (± 0.04) and characterizes the spatial distribution of the singularities, which contributes to the mean of the flux; $C_1 = 0.14$ is relatively high when compared to other geophysical fields, especially the volcanic albedo field (see below), implying a more isolated distribution of the present thermal radiative singularities equal or above C_1.

Finally, the non-conservation parameter H is related to the previous parameters by:

$$H = \frac{\beta - 1 + K(2, 1)}{2} = \frac{\beta - 1}{2} + \frac{C_1(2^{\alpha} - 2)}{2(\alpha - 1)} \tag{9}$$

The averaged H value is close to 0.65 (± 0.05), which is also higher than the corresponding volcanic albedo value, and demonstrates the smoother nature of the observed volcanic thermal field (see §4.2).

When compared to night-time images, the few daytime images analysed (see table 2) do not show any difference in the parameters C_1 and α, but they do show a slightly higher H value which we discuss below.

5. Comparison with other geophysical fields

The multifractal properties of various geophysical fields have been estimated by various authors. Figure 7 reveals the universal multifractal parameters found here and compares them with others in the literature. The Hawaiian volcanic thermal

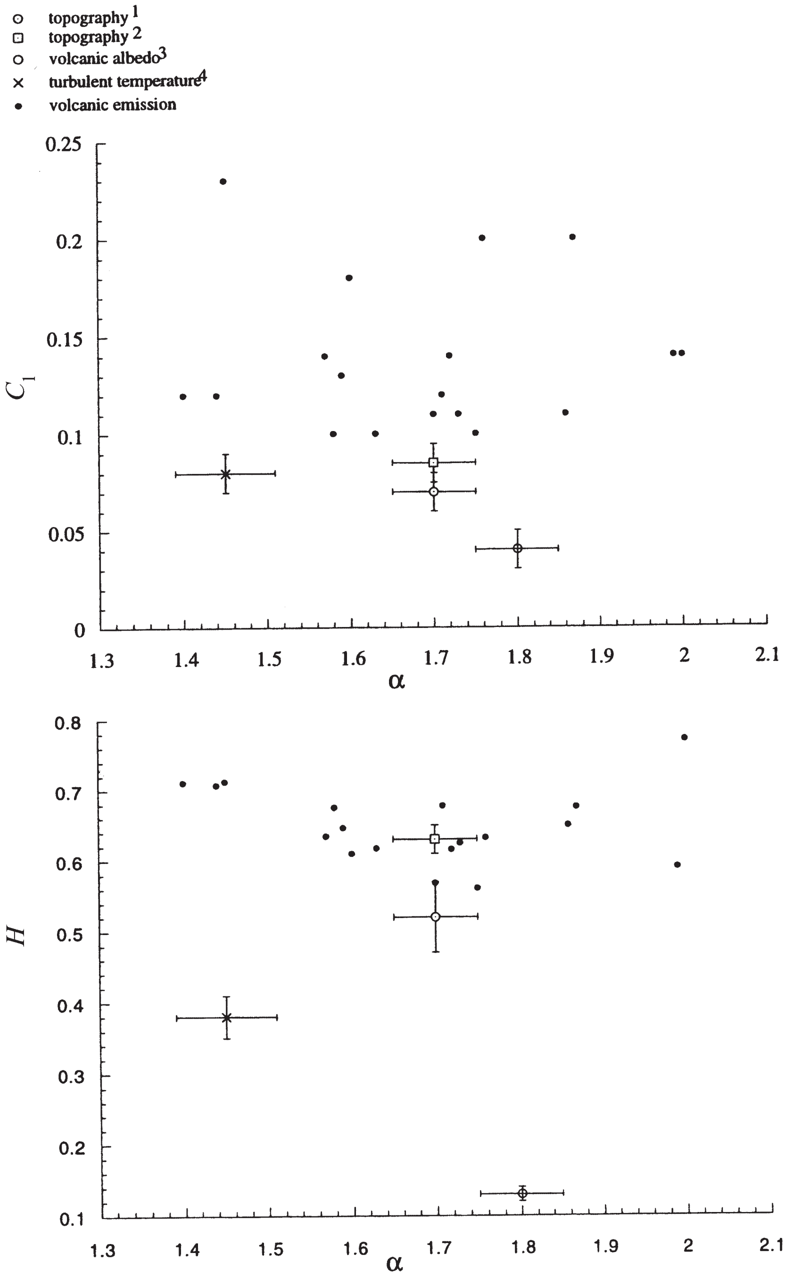

Figure 7. (*a*) Diagram of C_1 versus α for volcanic and non-volcanic fields; (*b*) diagram of H versus α for the same geophysical fields. (1) Pecknold *et al.* (1997); (2) Gagnon *et al.* (2003); (3) Laferrière and Gaonac'h (1999); (4) Schmitt *et al.* (1996).

emission field acquired for the present study has roughly the same high degree of multifractality (generally $\alpha > 1.5$) but is less conservative (higher H value) and shows a higher C_1 value than the volcanic albedo field. The difference in H between these two fields implies that the night-time thermal radiance field with its higher Hurst value ($H \approx 0.65$) is considerably smoother than the albedo field ($H \approx 0.13$). This difference is presumably a consequence of the distinct radiative transfer processes dominating the two bands. The albedo field is due to the reflection of the solar light on the volcanic surface and—since the basalt is fairly uniformly 'black'—is directly related to the local topographic gradient of the volcano. In contrast, the night-time thermal radiance field expresses the variability of the intensities (not to be confused with the amplitudes of the intensities) of the black body radiation—in this case largely produced by the volcanic activity, i.e. migration of the volcanic heat from the magmatic system to the surface on its topography. Comparison with the multifractal characteristics of the topography confirms the statistical relationship between the two volcanic fields: (1) the topography field has a degree of multifractality (α) close to that of both the volcanic thermal radiance field and the albedo fields; the H value of the topography (≈ 0.52, Pecknold *et al.* 1997; and ≈ 0.63, Gagnon *et al.* 2003) is close to that of the thermal radiance field while being much higher than the volcanic albedo field (≈ 0.13); (2) C_1 topographic value (≈ 0.07, Pecknold *et al.* 1997; and ≈ 0.085, Gagnon *et al.* 2003) lies between the albedo field ($C_1 \approx 0.04$) and the thermal field ($C_1 \approx 0.14$). This latter topographic C_1 parameter does not demonstrate a clear distinctive behaviour compared to the two volcanic fields (albedo and thermal) while the H values of the thermal and topographic fields seem more strongly associated. This may be due to the sensitivity of the C_1 parameter to the chosen geographic location as well as the presence of anisotropy in the field. Hence thermal, albedo and topography data over a region with similar resolutions will be needed to carefully clarify their statistical similarities/discrepancies. In any event, thermal C_1 and H values of the volcanic emission field are clearly higher than volcanic albedo values. This is in agreement with results found by Harvey *et al.* (2002), where a higher degree of volcanic activity in Hawaii has been associated with higher thermal C_1 and H parameters in the thermal infrared region while similar values were found between visible and thermal infrared for non-active areas.

6. Discussion

6.1. *Implications for temperatures and fluxes*

As indicated in figure 3, due to the sensor band, the thermal radiances and corresponding radiant temperatures are roughly linearly related over the relevant ranges. This means that if we ignore small variations in the emissivity, the multiscaling properties of the observed radiances and temperature fields are the same. However, it is of interest to estimate the radiative cooling (which is the total radiant energy flux) from the band observations. Let us assume constant emissivity and a Stefan–Boltzmann T^4 relation between temperature and total fluxes (F). In the case of homogeneous pixel at scale λ^{-1} then we obtain for a position vector $\mathbf{x}$:

$$F_\lambda(\mathbf{x}) \propto T_\lambda^4(\mathbf{x}) \tag{10a}$$

However, due to the strong multifractal sub-pixel variability, this relation does not hold at the pixel scale, only at the much smaller scale Λ^{-1}. We must instead consider the statistical average (indicated by $< >$) of fluxes F_Λ at the true very small sub-pixel homogeneity scale Λ^{-1} conditioned on the larger scale measurement T_λ. Using standard notation (figure 8), this conditional expectation for a flux F_λ given a measured T_λ can be written as (for simplicity we dropped the position vector in the expression of the stochastic variable F_λ): $\langle F_\lambda | T_\lambda \rangle$.

If the multifractal process is a conserved one (i.e. it is the direct result of a multiplicative cascade, $H=0$), the spatial average at resolution λ^{-1} can be estimated by the ensemble average at resolution Λ^{-1} so that: $F_\lambda | T_\lambda \approx \langle F_\Lambda | T_\lambda \rangle$; this is the value of the flux at resolution λ conditioned on the value of the temperature at resolution λ. The '$\approx$' includes a random factor which is of order unity if the corresponding moments converge. Finally, since $F_\Lambda \propto T_\Lambda^4$, we obtain:

$$F_\lambda | T_\lambda \propto \langle T_\Lambda^4 | T_\lambda \rangle \tag{10b}$$

We can now use the factorization property of the cascade to obtain:

$$\langle T_\Lambda^q | T_\lambda \rangle = T_\lambda^q \left(\frac{\Lambda}{\lambda} \right)^{K(q)} \tag{11}$$

(see Lovejoy *et al.* 2001 for details) and use $q=4$ ($K(q)$ is the usual multiscaling exponent; see equation (3)). This explicitly gives the bias factor due to the heterogeneity $(\Lambda/\lambda)^{K(4)}$ which is potentially significant since Λ/λ can be large (e.g. 10 m/1 cm $=10^3$). For example, using $C_1=0.14$, $\alpha=1.7$, $K(4)=1.3$, biases close to a factor of 10^3 would result if $H=0$. Due to smoothing implied by the large H value ($H\approx 0.65$), the actual bias will be considerably smaller; however, this does show that the effect of variability/heterogeneity over wide ranges can easily yield large effects. Hyperspectral data can also be interpreted in this framework using a kind of multifractal generalization of the multi-band method; we develop this idea elsewhere.

6.2. *The effect of daytime solar heating*

Another important result of our study is that both daytime and night-time images show multiscaling behaviour, mostly differing in their H (or β) value corresponding to a linear relation (power law filter) between the two. Hence, even if the daytime

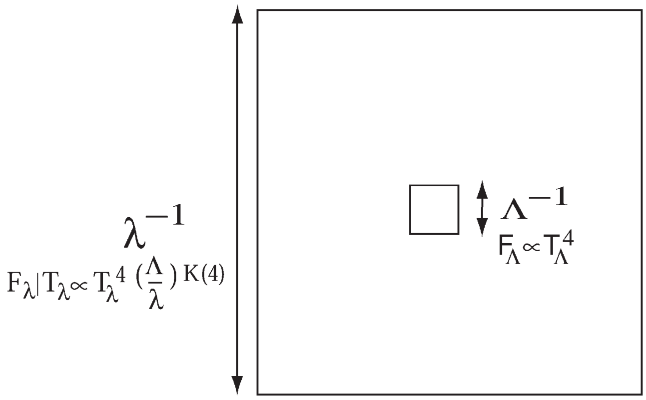

Figure 8. Schema of a heterogeneous pixel of size λ^{-1} with sub-pixel homogeneity at size Λ^{-1}. The total fluxes F at the homogeneous scale of Λ^{-1} and at the heterogeneous scale of λ^{-1} may be, respectively, deduced to be $F_\Lambda \propto T_\Lambda^4$ and $F_\lambda | T_\lambda \propto T_\lambda^4 (\Lambda/\lambda)^{K4}$.

thermal radiative field appears smoother than the night-time field we may easily relate the two fields—at least statistically—via a power filter. This has advantages since daytime monitoring may be easier but night-time images are more commonly used to estimate fluxes and the degree of activity on an active region (for example, it doubles the number of useful Landsat images). Figure 9 shows the result of power law filtering of two daytime images by the amount necessary (k^{-H} with $H=-0.1$) to obtain similar statistics (at all scales) to the night-time images. This result demonstrates the potential of using scaling properties of thermal fields to power law filter daytime images and to enhance the contrast of existing thermal volcanic anomalies present in the images without changing their general statistical properties except their roughness characteristics (through H values) at all spatial frequencies. Although this method generates 'simulations' of night-time imagery, further image by image analysis will be necessary to see whether or not the enhancement reveals the same anomalies as the night-time images.

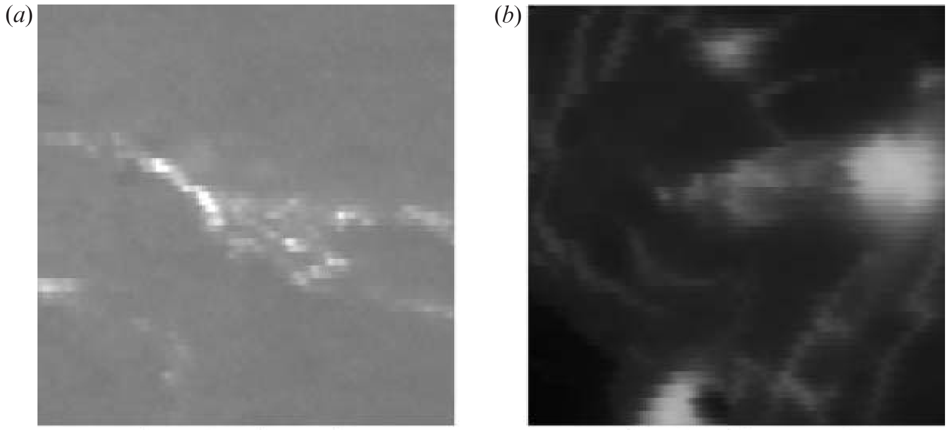

day-time lava tubes day-time lava pond

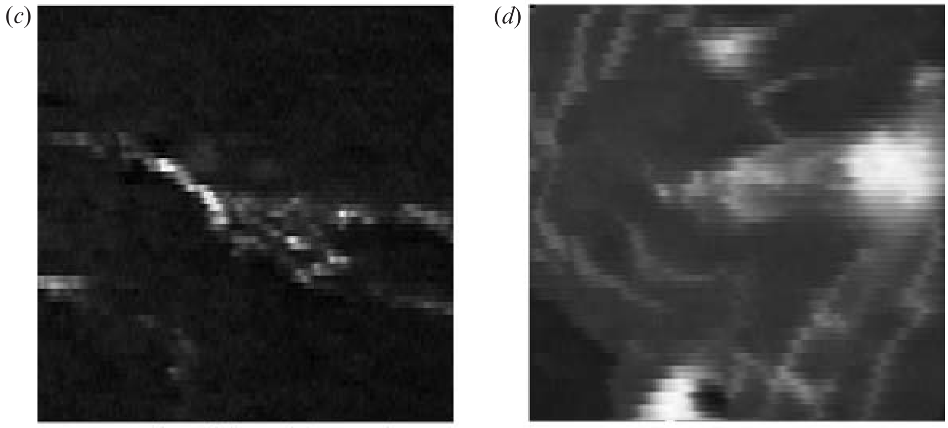

power law filtered lava tubes power law filtered lava pond

Figure 9. Daytime thermal images of (*a*) lava tubes and (*b*) lava pond. (*c*) Simulated night-time image (*a*) with a filter $H=-0.1$. (*d*) Simulated night-time image (*b*) with a filter $H=-0.1$.

7. Conclusions

Until now, remote data acquired at various resolutions have been limited (1) to qualitative results such as estimates of the highest temperatures on different active features and (2) the use of very few pixels to deduce the activity of a whole active region. Hence these studies provide a way to identify some general volcanic activity but cannot provide information and understanding of the nonlinear dynamics of the thermal radiative budget of the active surface. For example, in Harris and Stevenson (1997), a steady level of activity as inferred via the estimated radiative heat flux was observed on Vulcano between 1994 and 1995 while ground measurements suggest a displacement of the active fumarolic zones from the external rim into the centre of the Vulcano crater.

Our analyses respect the presence of such variability and interpret it as being an indirect result of an underlying scaling process. In such a model, the variability of the thermal radiative field increases in a power law way as we go to smaller scales, the statistics therefore having a simple scaling relation from one scale to another. In the present study, the volcanic surfaces of Kilauea volcano observed from helicopter—active in December 1995—exhibited thermal radiation fields which were highly variable over wide ranges of scale. These fields show scale-invariant symmetry properties which, for each image, we quantify over a range of scales $\approx 2^7$. Since the intrinsic image resolution varied by roughly a factor of 10^2, overall this covers a range of $>10^4$ in scale (4 cm to 770 m). The various active thermal fields—pahoehoe surface lava flows, lava tubes, lava ponds and skylights—all show a common scaling behaviour with a β value close to 2.0 (± 0.1). Furthermore, the thermal radiative field shows universal multifractal parameters, $\alpha \approx 1.7$ (± 0.2), $C_1 \approx 0.14$ (± 0.04), $H \approx 0.65$ (± 0.05), demonstrating that a monofractal approximation (corresponding to $\alpha = 0$) would not be accurate (except perhaps for characterizing the behaviour very close to the mean).

When compared to the topography and albedo fields, the Hawaiian thermal radiance field shows a similar degree of multifractality. Both remotely sensed volcanic fields are linked to the topography with distinct characteristics associated with different radiation interactions with the ground. If we assume that variations in albedo are purely due to roughness/topographic effects (i.e. for the albedo of volcanic surfaces to be roughly constant at the small homogeneous scale, as outlined in Laferrière and Gaonac'h (1999)), a direct relation between the topography and the albedo fields exists and simple models show that the former should have $H \approx 0$ with the same C_1, α as for the topography. Similarly, the volcanic thermally induced black body radiance field mimics the topography behaviour of the volcano, with their close C_1 and H characteristics. Moreover, our results clearly express the large difference between a field deduced from topography gradients to one associated directly to the topography including volcanic fractures and rifts. Due to strong heterogeneity, quantities such as heat fluxes cannot be inferred directly from the low resolution radiances; we show how large biases will result and, using multifractal conditional expectations, explain how to improve flux estimates.

More thermal studies have to be done after this preliminary work, on larger images, at both smaller and larger scales, in other spectral regions and with more sensitive instruments (higher dynamic range). In a companion paper, Harvey *et al.* (2002) compare the active Kilauea surface observed from various resolutions (1) simultaneously in different parts of the electromagnetic spectrum, (2) as well as active volcanic areas compared to inactive zones. Quantitative relations between the different mechanisms (thermal emission, reflection) observed in the bands are discussed in Harvey *et al.* (2002). Other volcanic regions will also have to be studied to confirm the universality of the radiative statistics as well as more constrain on the relations between associated fields (topography, albedo, thermal emission). Multifractal simulations (e.g. Pecknold *et al.* 1997) of the volcanic thermal field based on the parameters estimated here may help us understand the dynamics of lava flow emplacement, to determine the biases when using low-resolution radiances to estimate total fluxes (radiative cooling), and to exploit the multifractal statistics to develop new hyperspectral estimation methods. Finally, multiscaling properties of the emissivity of the Earth's surface are necessary in order to exploit this information for radiative flux estimates.

Acknowledgments

We would like to thank Y. Tessier and J.D. Stanway for technical support. We are grateful for assistance received in the field from P.A. Tremblay from Tremcour C^{ie} (Montreal). We thank L.P. Flynn and D. Pieri for helpful comments on an earlier version of this paper. This research has been funded by the National Sciences and Engineering Research Council of Canada and the Fonds pour la Formation de Chercheurs et d'Aide à la Recherche grants.

References

Bruno, B. C., and Taylor, G. J., 1995, Morphological identification of Venusian lavas. *Geophysical Research Letters*, **22**, 1897–1900.

Bruno, B. C., Taylor, G. J., Rowland, S. K., and Baloga, S. M, 1994, Quantifying the effect of rheology on lava-flow margins using fractal geometry. *Bulletin of Volcanology*, **56**, 193–206.

Dubois, J., and Cheminée, J. L., 1993, Les cycles éruptifs du Piton de la Fournaise: analyse fractale, attracteurs, aspects déterministes. *Bulletin de la Société géologique de France*, **164**, 3–16.

Flynn, L. P., and Mouginis-Mark, P. J., 1994, Temperature of an active lava channel from spectral measurements, Kilauea Volcano, Hawaii. *Bulletin of Volcanology*, **56**, 297–301.

Flynn, L. P., Mouginis-Mark, P. J., and Horton, K. A., 1994, Distribution of thermal areas on an active lava flow field: Landsat observations of Kilauea, Hawaii, July, 1991. *Bulletin of Volcanology*, **56**, 284–296.

Flynn, L. P., Harris, A. J. L., Rothery, D. A., and Oppenheimer, C., 2000, High-spatial-resolution thermal remote sensing of active volcanic features using Landsat and hyperspectral data. In *Remote Sensing of Active volcanoes*, edited by P. J. Mouginis-Mark, J. A. Crisp and J. H. Fink, *Geophysical Monograph Series*, vol. 116, pp. 161–177.

Gagnon, J. S., Lovejoy, S., and Schertzer, D., 2003, Multiscaling surfaces and terrestrial topography, *Europhysics Letters*, in press.

Gaonac'h, H., Lovejoy, S., and Stix, J., 1992, Scale invariance of basaltic lava flows and their fractal dimensions. *Geophysical Research Letters*, **19**, 785–788.

Gaonac'h, H., Lovejoy, S., Stix, J., and Schertzer, D., 1996a, A scaling growth model for bubbles in basaltic lava flows. *Earth and Planetary Science Letters*, **139**, 395–409.

Gaonac'h, H., Stix, J., and Lovejoy, S., 1996b, Scaling effects on vesicule shape, size and heterogeneity of lavas from Mount Etna. *Journal of Volcanology and Geothermal Research*, **74**, 131–153.

Gaonac'h, H., Vandemeulebrouck, J., Stix, J., and Halbwachs, M., 1994, Thermal infrared satellite measurements of volcanic activity at Stromboli and Vulcano. *Journal of Geophysical Research*, **99**, 9477–9485.

Glaze, L., Francis, P. W., and Rothery, D. A, 1989, Measuring thermal budgets of active volcanoes by satellite remote sensing, *Nature*, **338**, 144–146.

HARRIS, A. J. L., and STEVENSON, D. S., 1997, Thermal observations of degassing open conduits and fumaroles at Stromboli and Vulcano using remotely sensed data. *Journal of Volcanology and Geothermal Research*, **76**, 175–198.

HARRIS, A. J. L., BUTTERWORTH, A. L., CARLTON, R. W., DOWNEY, I., MILLER, P., NAVARRO, P., and ROTHERY, D. A., 1997, Low-cost volcano surveillance from space: case sudies from Etna, Krafla, Cerro Negro, Fogo, Lascar and Erebus. *Bulletin of Volcanology*, **59**, 49–64.

HARRIS, A. J. L., FLYNN, L. P., KESZTHELYI, L., MOUGINIS-MARK, P. J., ROWLAND, S. K., and RESING, J. A., 1998, Calculation of lava effusion rates from Landsat TM data. *Bulletin of Volcanology*, **60**, 52–71.

HARRIS, A. J. L., FLYNN, L. P., DEAN, K., PILGER, E., WOOSTER, M., OKUBO, C., MOUGINIS-MARK, P., GARBEIL, H., THORNBER, C., DE LA CRUZ-REYNA, S., ROTHERY, D., and WRIGHT, R., 2000, Real-time satellite monitoring of volcanic hot spots. In *Remote Sensing of Active volcanoes*, edited by P. J. Mouginis-Mark, J. A. Crisp and J. H. Fink, *Geophysical Monograph Series*, vol. 116, pp. 139–159.

HARVEY, D. A., GAONAC'H, H., LOVEJOY, S., STIX, J., and SCHERTZER, D., 2002, Multifractal characterization of remotely sensed volcanic features: a case study from Kilauea volcano, Hawaii. *Fractals*, **10**, 265–274.

KAHLE, A. B., GILLESPIE, A. R., ABBOTT, E. A., ABRAMS, M. J., WALKER, R. E., HOOVER, G., and LOCKWOOD, J. P., 1988, Relative dating of Hawaiian lava flows using multispectral thermal infrared images: a new tool for geologic mapping of young volcanic terranes. *Journal of Geophysical Research*, **93**, 15 239–15 251.

LAFERRIÈRE, A., and GAONAC'H, H., 1999, Multifractal properties of visible reflectance fields from basaltic volcanoes. *Journal of Geophysical Research*, **104**, 5115–5126.

LAVALLÉE, D., LOVEJOY, S., SCHERTZER, D., and LADOY, P., 1993, Nonlinear variability of landscape topography: multifractal analysis and simulation. In *Fractals in Geography*, edited by L. De Cola and N. Lam (London: Prentice Hall), pp. 158–192.

LOVEJOY, S., and SCHERTZER, D., 1995, How bright is the coast of Brittany? In *Fractals in Geoscience and Remote Sensing*, edited by G. Wilkinson, I. Kanellopoulos and J. Mégier, ECSC-EC-EAEC, Brussels, pp. 102–151.

LOVEJOY, S., SCHERTZER, D., TESSIER, Y., and GAONAC'H, H., 2001, Multifractal and resolution dependent remote sensing algorithms: the example of ocean colour. *International Journal of Remote Sensing*, **22**, 1191–1234.

OPPENHEIMER, C., 1991, Lava flow cooling estimated from Landsat Thematic Mapper infrared data: the Lonquimay eruption (Chile, 1989). *Journal of Geophysical Research*, **96**, 21 865–21 878.

OPPENHEIMER, C., ROTHERY, D. A., and FRANCIS, P. W., 1993a, Thermal distributions at fumarole fields: implications for infrared remote sensing of active volcanoes. *Journal of Volcanology and Geothermal Research*, **55**, 97–115.

OPPENHEIMER, C., FRANCIS, P. W., ROTHERY, D. A., and CARLTON, R. W. T., 1993b, Infrared image analysis of volcanic thermal features: Làscar Volcano, Chile, 1984–1992. *Journal of Geophysical Research*, **98**, 4269–4286.

PARISI, G., and FRISCH, U., 1985, A multifractal model of intermittency. In *Turbulence and Predictability in Geophysical Fluid Dynamics and Climate Dymamics*, edited by R. B. Ghil and G. Parisi (Amsterdam: North Holland), pp. 84–88.

PECKNOLD, S., LOVEJOY, S., SCHERTZER, D., and HOOGE, C., 1997, Multifractals and resolution dependence of remotely sensed data: GSI and GIS. In *Scale in Remote Sensing and GIS*, edited by D. A Quattrochi and M. F. Goodchild (Boca Raton, FL: CRC Press), pp. 361–394.

ROTHERY, D. A., FRANCIS, P. W., and WOOD, C. A., 1988, Volcano monitoring using short wavelength infrared data from satellites. *Journal of Geophysical Research*, **93**, 7993–8008.

REALMUTO, V. J., HON, K., KAHLE, A. B., ABBOTT, E. A., and PIERI, D. C., 1992, Multispectral thermal infrared mapping of the 1 October 1988 Kupaianaha flow field, Kilauea volcano, Hawaii. *Bulletin of Volcanology*, **55**, 33–44.

REALMUTO, V. J., SUTTON, A. J., and ELIAS, T., 1997, Multispectral thermal infrared mapping of sulfur dioxide plumes: a case study from the East Rift Zone of Kilauea Volcano, Hawaii. *Journal of Geophysical Research*, **102**, 15 057–15 072.

Schmitt, F., Schertzer, D., Lovejoy, S., and Brunet, Y., 1996, Multifractal temperature and flux of temperature variance in fully developed turbulence. *Europhysics Letters*, **34**, 195–200.

Schmitt, F., Schertzer, D., Lovejoy, S., and Marchal, P., 1997, Multifractal analysis of satellite images: towards an automatic segmentation. *Proceedings, Fractals in Engineering, Arcachon, France, 25–27 June 1997* (Rocquencourt: INRIA).

Schertzer, D., and Lovejoy, S., 1987, Physical modeling and analysis of rain and clouds by anisotropic scaling of multiplicative processes. *Journal of Geophysical Research*, **92**, 9693–9714.

Schertzer, D., and Lovejoy, S., 1991, Nonlinear geodynamical variability: multiple singularities, universality and observables. In *Non-Linear Variability in Geophysics: Scaling and Fractals*, edited by D. Schertzer and S. Lovejoy (Dordrecht: Kluwer), pp. 41–82.

Schertzer, D., and Lovejoy, S., 1995, Standard and advanced multifractal techniques in remote sensing. In *Fractals in Geosciences and Remote Sensing*, edited by G. Wilkinson, I. Kanellopoulos and J. Mégier (Luxembourg: Office for Official Publications of the European Communities), pp. 11–40.

Schertzer, D., Lovejoy, S., Schmitt, F., Chigirinskaya, Y., and Marsan, D., 1997, Multifractal cascade dynamics and turbulent intermittency. *Fractals*, **5**, 427–471.

Wooster, M. J., and Kaneko, T., 1998, Satellite thermal analyses of lava dome effusion rates at Unzen Volcano, Japan. *Journal of Geophysical Research*, **103**, 20 935–20 947.